



Analysis of thermal and electrical conductivity properties of Al substitution $\text{LiHf}_2(\text{PO}_4)_3$ chemical solid electrolyte

Tasiu Zangina¹ · Jumiah Hassan^{1,2} · Raba'ah Syahidah Azis^{1,2} · Khamirul Amin Matori^{1,2} · Tan Foo Khooon² · Makiyyu Abdullahi Musa¹

© Springer Nature Switzerland AG 2019

Abstract

Lithium ion conducting solid electrolytes, lithium aluminum hafnium phosphate ($\text{Li}_{1+x}\text{Hf}_{2-x}\text{Al}_x(\text{PO}_4)_3$, $x=0-0.75$) are prepared via solid state synthesis technique. Thermo-gravimetric analysis indicates that the thermal decomposition and thermal stability of the reaction mixture is generally affected by a high content of x value substitution. It can be observed that as x content or aluminum substitution increases, the thermal decomposition and thermal stability increase which leads to the sample formation towards higher temperature. For X-ray diffraction analysis, the Rietveld refinement analysis indicates the presence of different types of secondary phases as aluminum content increases. Single phase of lithium hafnium phosphate ($\text{LiHf}_2(\text{PO}_4)_3$) is only achievable in the absence of any aluminum substitution. Furthermore, for the lithium ionic conductivity, the findings indicate that conductivity increases with increase in x substitution in lithium aluminum hafnium phosphate. The highest AC conductivity is observable in the sample with composition $x=0.25$ of about $2.5 \times 10^{-3} \Omega^{-1}\text{m}^{-1}$ with low activation energy 0.36 eV. The present studies recommend the sample with composition $x=0.25$ ($\text{Li}_{1.25}\text{Hf}_{1.75}\text{Al}_{0.25}(\text{PO}_4)_3$) to be a future solid electrolyte material for battery applications.

Keywords NASICON-type · $\text{Li}_{1.25}\text{Hf}_{1.75}\text{Al}_{0.25}(\text{PO}_4)_3$ · Structural · Thermal behavior · Ionic conductivity properties

1 Introduction

Lithium based superionic conductors (NASICON-type) analogs to Sodium Zirconia Phosphate NZP are known to be fast ionic conductors due to the high mobility of Li^+ ions in its structure. It is a rhombohedra crystal system with several interesting features and potential applications; which include high ionic conductivity, low thermal expansion coefficient [1] and thermodynamic stability [2]. It has a unique property of varied ionic substitution in its structure that could accommodate many elements in the periodic table in its lattice without altering the basic structure. Superionic conductors based on lithium titanium phosphate ($\text{Li-Ti}_2(\text{PO}_4)_3$) [3] are the most promising

compounds studied in recent decades. Most researches on superionic conductors were done in the titanium system $\text{LiTi}_2(\text{PO}_4)_3$ (LTP). The small size of the Ti^{4+} cations makes the size of the site's in the channels more appropriate for lithium cations [4, 5], but instability was reported in the LTP compounds due to the reduction of Ti^{4+} to Ti^{3+} by the Li^+ ion which restricts their application in solid state electrolyte [5, 6]. However, it has been reported that Hf^{4+} ion is more stable towards lithium metal and reductive gasses than the Ti^{4+} ion, which is an additional advantage for battery applications [6].

Lithium hafnium phosphate $\text{LiHf}_2(\text{PO}_4)_3$ (LHP) material crystallizes in NASICON-type structure, but there is the problem of the material undergoing a top tactic and

✉ Tasiu Zangina, tasiuzangina@gmail.com; Jumiah Hassan, jumiah@upm.edu.my; Raba'ah Syahidah Azis, rabaah@upm.edu.my; Khamirul Amin Matori, khamirul@upm.edu.my; Tan Foo Khooon, fookhoon1202@hotmail.com; Makiyyu Abdullahi Musa, makiyyu37@gmail.com | ¹Department of Physics, Faculty of Science, Universiti Putra Malaysia, 43400 UPM Serdang, Selangor, Malaysia. ²Institute of Advanced Technology, Universiti Putra Malaysia, 43400 UPM Serdang, Selangor, Malaysia.



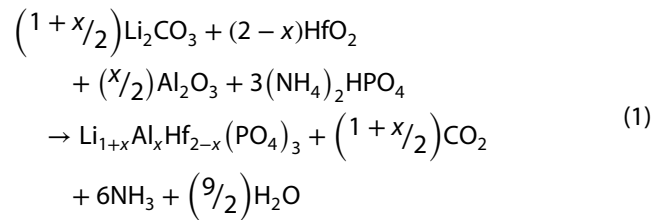
reversible phase transition at low temperature [7]. Few works have been reported on LHP on its poor sinterability and controversial phase transition at low temperature during synthesis [8]. To our knowledge, aluminum (Al) substitution in LHP was only reported by Chang et al. [6] using spark plasma sintering technique (SPS). The effect of SPS technique and the ionic substitution with aluminum ion were investigated based on the material densification to enhance the Li^+ ion conductivity [6], but the thermal behavior of the aluminum-substituted composition was not fully discussed. Thermal analysis is essential in any sample preparation. Analysis of the thermal behavior of a certain compound indicates its thermal stability range within which it exhibits all the phase transformations [9].

In this work, a series of characterizations were carried out beginning with synthesis and structural characterization of $\text{Li}_{1+x}\text{Hf}_{2-x}\text{Al}_x(\text{PO}_4)_3$ ($x=0-0.75$) using XRD and FTIR techniques. The thermal behavior of the compositions was studied, and the phase composition was examined with the change in the x content and also the effect of Al in LHP basic compound from room temperature to 800°C using TGA techniques. Similarly, the effect of x substitution on the electrical conductivity of the as-prepared samples is also investigated.

2 Experimental techniques

2.1 Synthesis

The microcrystalline materials, lithium aluminum hafnium phosphate ($\text{Li}_{1+x}\text{Hf}_{2-x}\text{Al}_x(\text{PO}_4)_3$, ($x=0, 0.2, 0.25, 0.3, 0.4, 0.5$ and 0.75) were synthesized by conventional solid-state synthesis technique. Materials of AR grade were used as basic starting materials, Li_2CO_3 (99% Alfa Aesar), HfO_2 (99.9% Alfa Aesar), $(\text{NH}_4)_2\text{HPO}_4$ (98% Alfa Aesar), and Al_2O_3 (96% Strem) in a stoichiometric amount. Seven compounds according to the x values were prepared. The stoichiometry mixture is mixed in methanol and ball-mixed for 24 h and then dried in an oven for 24 h. The dried mixtures were calcined in an alumina crucible at 700°C for 3 h at the heating rate of 2°C min^{-1} in air in order to release volatile products such as carbon dioxide, ammonia and also water content. The overall chemical reaction is given in Eq. 1. The calcined powders (with uniform size) were made into pellets by pressing uniaxially at 200 MPa. Sintering was carried out at 1100°C for 3 h at the same heating rate i.e. 2°C min^{-1} .



2.2 Measurement and characterization procedures

Virgin powders of the specimen (of about 16 mg) were used for TGA/DTG analysis after ball mixing for 24 h. The thermogravimetric analysis (TGA) was carried using TGA machine Metler Toledo Brand, (Model number TGA/DSC HT). The measurements were carried out in air from room temperature to 800°C at a heating rate of 10 K min^{-1} .

The phases and structural compositions of the as-prepared samples were confirmed by X-ray diffraction analysis using an XRD machine, Philips X'pert diffractometer model 7602 EA Almelo with Cu K α radiation source with $\lambda=1.5418\text{ \AA}$. The measurement was carried out at room temperature with 2θ scanning range from 10 to 60° . The interpretation and data analysis of the XRD patterns were conducted for the entire prepared samples sintered at 1100°C based on the database of the Inorganic Crystal Structure Database (ICSD) using High Score X'pert plus software version 3.0e. The lattice parameters and unit cell volume of LAHP were obtained from the software after the Rietveld analysis.

Experimental and theoretical densities of the materials were measured; Archimedes procedure was used for the experimental density whereas theoretical or X-ray density ρ_{xrd} was obtained using Eq. (2)

$$\rho_{\text{xrd}} = \frac{nM}{VN_A} \quad (2)$$

where V is the unit cell volume calculated from the XRD lattice constant using a software, M is the molecular mass of the as prepared samples as shown in Table 1, n is the number of atoms at the vertices per unit cell (for hexagonal structure n is 6) and N_A is Avogadro's number.

The functional compositions of the phosphate for LAHP were confirmed from the FTIR spectra. The method is used to identify chemical components, bonds and functional groups of the materials. The vibrational modes of PO_4 were assigned in the intervals of the standard group vibrations. The measurement was carried out using Perkin Elmer Spectrum 100 Series spectrophotometer (Waltham MA).

Table 1 Percentage total mass loss, residue and the stability temperature of LAHP

x content	Li _{1+x} Hf _(2-x) Al _x (PO ₄) ₃ samples	Molecular weight (M) (g/mol)	Mass loss (%)	Residue (%)	Thermal stability temperature (°C)
0	LiHf ₂ (PO ₄) ₃	648.830	20.20	79.80	345.0
0.2	Li _{1.2} Hf _{1.8} Al _{0.2} (PO ₄) ₃	614.916	20.70	79.30	376.5
0.25	Li _{1.25} Hf _{1.75} Al _{0.25} (PO ₄) ₃	612.730	20.60	79.40	390.6
0.3	Li _{1.3} Hf _{1.7} Al _{0.3} (PO ₄) ₃	605.524	20.50	79.50	419.0
0.4	Li _{1.4} Hf _{1.6} Al _{0.4} (PO ₄) ₃	591.022	21.20	78.80	407.0
0.5	Li _{1.5} Hf _{1.5} Al _{0.5} (PO ₄) ₃	576.560	22.71	77.30	472.5
0.75	Li _{1.75} Hf _{1.25} Al _{0.75} (PO ₄) ₃	540.425	22.40	77.60	477.5

For electrical conductivity measurements, the surfaces of the sintered pellets were coated with silver paint to function as electrodes and the dimension of the pellet was recorded. The data was obtained using Agilent 4294A precision impedance analyzer in the frequency range 40 Hz–1 MHz at room temperature. The AC conductivity measurement was elucidated using the Jonscher's power law which is used to explain the frequency dependence of AC conductivity and also gives the total conductivity contribution of both AC and DC conductivities as in Eq. (3).

$$\sigma(\omega) = \sigma(o) + A\omega^n \quad (3)$$

where A is the pre-exponential factor (AC coefficient) which is temperature dependent, $\sigma(o)$ is the DC conductivity which is observed at low frequency and it is temperature dependent and n is the frequency exponent.

DC conductivity is the direct current conductivity which cannot be measured directly in polycrystalline materials due to the polarization effect that exist at the sample-electrode interface. However, impedance analysis technique which involves equivalent circuit modeling was employed to analyze and estimate the magnitude of the DC conductivity, σ_{dc} of the grain and grain boundary effects using Eqs. (4) and (5) for both grain (σ_g) and grain boundary conductivities (σ_{gb}) respectively. These are considered as sigma DC estimation from the AC measurement [10]. The analysis of equivalent circuit was carried out using Nova software (version1.11.1) to fit the Nyquist plot to determine the impedance of each sample. The circuit modeling involved mathematical technique which was used to fit the Nyquist plot via Eqs. (6) and (7);

$$\sigma_g = \frac{t}{AR_g} \quad (4)$$

$$\sigma_{gb} = \frac{t}{AR_{gb}} \quad (5)$$

where t is the thickness of sample, A the area of the coated surface and R_g , R_{gb} are the grain and grain boundary resistance respectively. The complex impedance constitutes the

$$Z' = \frac{R_g}{[1 + (\omega R_g C_g)^2]} + \frac{R_{gb}}{[1 + (\omega R_{gb} C_{gb})^2]} \quad (6)$$

and

$$Z'' = \frac{\omega R_g^2 C_g}{[1 + (\omega R_g C_g)^2]} + \frac{\omega R_{gb}^2 C_{gb}}{[1 + (\omega R_{gb} C_{gb})^2]} \quad (7)$$

where Z' and Z'' are the real and imaginary parts of the complex impedance respectively. R_g is grain-interior resistance, R_{gb} is the grain boundary resistance, ω is the angular frequency and C_g and C_{gb} are the capacitance of grain and grain boundary respectively. The activation energy of the Li⁺ ion was evaluated using Arrhenius relation Eq. (8).

$$\sigma T = \sigma_o \exp\left(\frac{-E_a}{K_B T}\right) \quad (8)$$

where σ is the DC conductivity, T is the temperature in Kelvin, σ_o is the pre-exponential factor, E_a is the activation energy and K_B is the Boltzmann's constant.

3 Results and discussion

3.1 TGA/DTG analysis

Figure 1 shows the TGA process for the thermal decomposition and stability behavior of the stoichiometric compositions Li_{1+x}Hf_{2-x}Al_x(PO₄)₃ $x=0, 0.2, 0.25, 0.3, 0.4, 0.5$ and 0.75 heated from room temperature to 800°C . It is clear that the samples showed the same trend with the same characteristic curves in both TGA and DTG plots in Fig. 2 but the temperature at which the materials achieved threshold stability increases linearly with x -substitution from $x=0$ to $x=0.75$. Each curve exhibited five temperature domains with different mass loss occurring at various temperature ranges. In each plot, the first mass loss

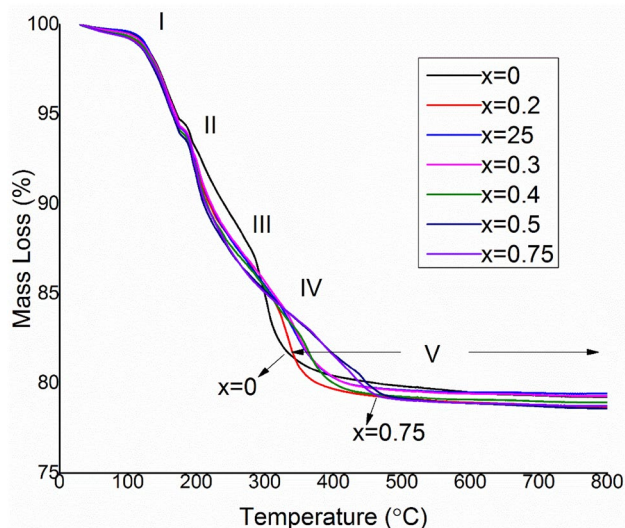


Fig. 1 TGA curves for the overall effect of increasing x-substitution in $\text{Li}_{1+x}\text{Hf}_{2-x}\text{Al}_x(\text{PO}_4)_3$ ($x=0-0.75$) with various stoichiometric composition on thermal decomposition and stability

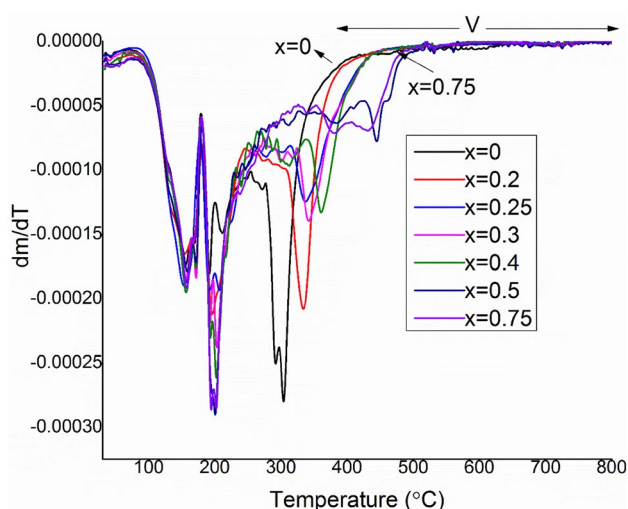


Fig. 2 DTG plots of $\text{Li}_{1+x}\text{Hf}_{2-x}\text{Al}_x(\text{PO}_4)_3$ ($x=0-0.75$) with various stoichiometric composition indicating the peaks of decomposition and stability temperature

in region I–II is attributed to the evaporation of moisture. The second and third weight loss in regions II–III is due to the stage decomposition of ammonium group that is supported more clearly by the DTG curve shown in Fig. 2 for each plot. The last mass loss occurred in region IV which is attributed to the decomposition of lithium carbonate (Li_2CO_3) which releases CO_2 gas. Region V is associated with complete chemical decomposition for the formation of the compounds beyond which the material maintained stability. These are in agreement with TGA results

reported by Savitha et al. [11] in the study of thermal analysis of $\text{Li}_2\text{AlZr}(\text{PO}_4)_3$. A similar trend was also reported [12] for $\text{Na}_{1+x}\text{Zr}_2\text{Si}_x\text{P}_{3-x}\text{O}_{12}$ prepared using co-precipitation method [13]. The results obtained in this study is quite different from that has already been reported [14] in which the substitutions of Hf^{4+} involved Cr and Fe ions in the crystalline materials. In their study, the sample’s crystallinity was observed to be stable at high temperature between room temperature to $1100\text{ }^\circ\text{C}$ and there was no mass loss.

Table 1 depicts the total mass loss, the residue and the temperature stability of each composition of $\text{Li}_{1+x}\text{Al}_x\text{Hf}_{2-x}(\text{PO}_4)_3$ with $x=0, 0.2, 0.25, 0.3, 0.4, 0.5$ and 0.75 . It can be seen that the percentage of total mass loss increases as the x substitution is increased in the reaction mixture. Another observation is that increase in the x value, increases the stability temperature which leads the sample formation towards higher temperature. This is possibly due to the higher content of carbonate which produces more carbon dioxide as the end product. The effect of Al substitution is also noticed from Table 1, which shows that as the x content increases the molecular weight of the as-prepared LAHP is observed to decrease. This is due to the decrease in the weight when a smaller radius and less atomic weight material are introduced into the system. The radius of Al and its atomic weight is less than that of the substituted hafnium.

In a similar analysis reported by Ahamdu et al. [9], the thermal analysis of $\text{Na}_{1-x}\text{Li}_x\text{Zr}_2(\text{PO}_4)_3$ was conducted with a lighter ion (lithium ion) substitution in the system. The report indicated that as the content of lithium ion increases, the percentage of mass loss decreases which may be associated with very low weight and small size of the substituted lithium ions.

Thus, for the un-substituted composition ($x=0$), a total mass loss of 20.20% was observed from room temperature to $800\text{ }^\circ\text{C}$ as illustrated in Fig. 1 and Table 1 where 4.20% weight loss was observed in region I (onset region) which is the initial mass loss, 10.87% mass loss in regions II and III and approximately 5.13% weight loss in region IV which is the offset region beyond which stability is achieved suggesting a complete chemical decomposition of the mixture. Higher percentage weight loss was observed in regions I and II. The TG curves indicated that LHP ($x=0$) start attaining stability at around $345\text{ }^\circ\text{C}$. The DTG peaks in Fig. 2 confirm all the decomposition processes occurring in the TG curve. Similar behavior was observed in the TG analysis of $\text{Na}_{1-x}\text{Li}_x\text{Zr}_2(\text{PO}_4)_3$ [15] in terms of mass loss in the regions I, II, III, and IV.

The curves for compositions $x=0.2, 0.25, 0.3,$ and 0.4 are equally shown in Fig. 1. All the curves exhibited almost similar behavior with respective average overall mass loss. The trend of the curves was observed to be similar as in

the case of $x=0$ but the temperature of stability changed for each sample as tabulated in Table 1.

For $x=0.5$, the respective mass losses were obtained as 4.04%, 13.24% and 4.43% in the regions as shown in Fig. 1 with the total mass loss of 22.71%. Similarly, it was observed there is further increase in the rate of mass loss as x -content increases in the system. The corresponding temperature of stability also increases further to 472.5 °C from regions III–IV. Similar behavior was observed for $x=0.75$ with the same rate of mass loss with increasing temperature as shown in Fig. 1 and Table 1 which are clearly confirmed by DTG plots in Fig. 2.

3.2 Structural analysis

Figure 3 shows the XRD diffraction patterns of all the sintered samples $\text{Li}_{1+x}\text{Al}_x\text{Hf}_{2-x}(\text{PO}_4)_3$ ($x=0, 0.2, 0.25, 0.3, 0.4, 0.5$ and 0.75). The Rietveld refinement analysis illustrates the various phases present in each compositions and the effect of Aluminum substitution into the basic compound LHP. It is indicated by the Rietveld analysis that the assumed crystal system is trigonal type structure with hexagonal axes belonging to $R\bar{3}c$ space group which proved the formation of NASICON-type LAHP.

The XRD results of unsubstituted LHP shows the sample powder sintered at 1100 °C for 3 h exhibited single

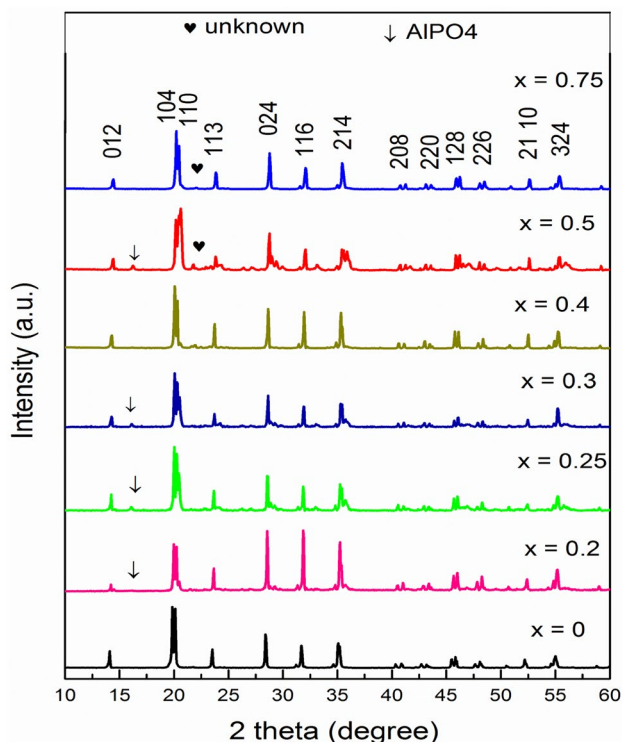


Fig. 3 X-Ray diffraction patterns of $\text{Li}_{1+x}\text{Hf}_{2-x}\text{Al}_x(\text{PO}_4)_3$ ($x=0-0.75$) with various composition sintered at 1100 °C

Table 2 Effect of Al substitution on lattice parameters, unit cell volume, and density of LAHP

x content	Unit cell parameters			Experimental density (g/cm ³)	Theoretical density (g/cm ³)
	a=b (Å)	c (Å)	V (Å ³)		
0	8.82479	22.01741	1484.93	4.134	4.354
0.2	8.80838	21.96727	1476.04	3.982	4.183
0.25	8.80822	21.96545	1475.87	3.895	4.133
0.3	8.80774	21.96717	1475.82	3.876	4.120
0.4	8.80813	21.96670	1475.96	3.865	3.988
0.5	8.80535	21.94779	1473.72	3.836	3.884
0.75	8.80926	21.95696	1475.64	3.401	3.634

phase with no secondary phases as reported elsewhere [16]. The unit cell volume and lattice parameters of the LHP analyzed are shown in Table 2 and the parameters are found to be in close agreement with the data reported by Chang et al. [17, 18] where $a=b=8.8285$ Å, $c=22.0190$ Å and $V=1484.40$ Å³.

For the Al substituted $x=0.2$, only one secondary phase was observed which is AlPO_4 corresponding to ICSD database 98-010-3915. However, as Al substitution is increased more Al secondary phases were detected. For compositions $x=0.25$ and 0.3 , other phases were observed; Berlinite (AlPO_4) corresponding to ICSD database 98-002-2357, AlPO_D corresponding to ICSD database 98-002-6723 and Aluminum Phosphate (AlPO_4) corresponding to ICSD database 98-002-6280. An additional of two more secondary phases were detected for $x=0.4$ and $x=0.5$ which include; AlPO_{-31} , with ICSD database 98-002-9743 and AlPO_{-8} with ICSD database 98-002-9742. As the number of Al content increases, the number of secondary phases also increases. More phases were observed for $x=0.75$. These include lithium Cantena Phosphate (LiPO_3) with ICSD database 98-000-6328 and AlPO_{-54} with ICSD database 98-002-3820 from the Rietveld analysis.

The effect of Al substitution on the lattice parameters, unit cell volume, and the densities is tabulated in Table 2. The values of the lattice constants were observed to decrease due to the Al substitution in the basic structure of the material and this is attributed to the shorter ionic radius of the substituting Al^{3+} ion (0.54 Å) compare to that of the substituted Hf^{4+} ion (0.71 Å). According to [19] a limiting difference of radii = 0.1 Å between the ionic radii is considered a good criterion for the forming a solid solution, this limit has been considerably exceeded in the present solid solutions and results in the formation of the secondary phases. Experimental and theoretical densities are tabulated in Table 2. All the experimental densities are more than 90% of the theoretical densities and this may improve the densification of the samples for higher ionic conductivity. A similar observation was also reported [6].

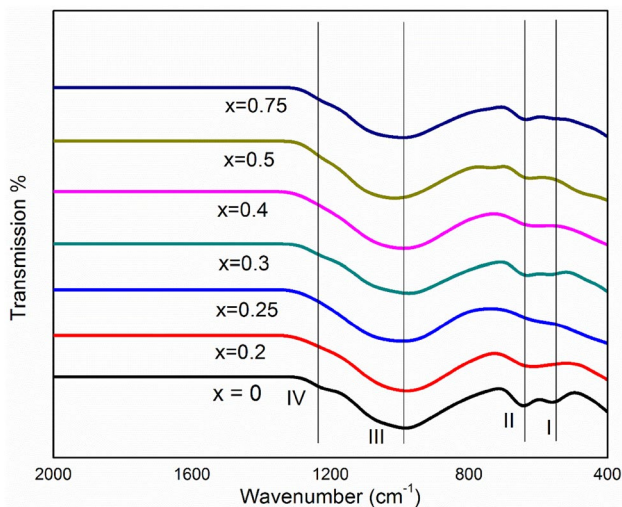


Fig. 4 FTIR spectra of $\text{Li}_{1+x}\text{Hf}_{2-x}\text{Al}_x(\text{PO}_4)_3$ ($x=0-0.75$) with different compositions sintered at $1100\text{ }^\circ\text{C}$

3.3 Functional group and vibrational analysis

The quality of the as-prepared samples was obtained using the Fourier-transform infrared analysis. Figure 4 depicts the FTIR spectra of $\text{Li}_{1+x}\text{Al}_x\text{Hf}_{2-x}(\text{PO}_4)_3$ for $x=0, 0.2, 0.25, 0.3, 0.4, 0.5$ and 0.75 which showed strong bending vibrations and stretching modes at various positions of the vibration band. The FTIR technique has advantages in identifying phases formed in a compound, structural exposition and functional group identification. It was reported that the spectra obtained from the FTIR for a NASICON-type compound are dominated by strong overlapping intermolecular PO_4^{3-} stretching modes of vibration which are expected to be within the range of $1300-700\text{ cm}^{-1}$ [20]. It can be seen that region I is associated with asymmetry stretching vibration band corresponding to the wavenumber $1100-1227\text{ cm}^{-1}$ while region II is due to the symmetry stretching vibrations of the PO_4^{3-} anions which is within the wavenumber $900-1000\text{ cm}^{-1}$. However, the observed absorption bands in region III from 643 to 750 cm^{-1} are assigned to the symmetry stretching vibration of P–O–P and region IV is the absorption band in the range $553-630\text{ cm}^{-1}$ due to the asymmetry bending vibration modes of O–P–O bonds. Similar behavior for NASICON-type materials were also reported [21–23]. In another observation, the modes slightly shifted towards higher wave number as Al content is increased in the basic LHP structure. This is attributed to the smaller atomic number of aluminum compared to the substituted hafnium atomic number. It was reported that absorption modes shift to higher wavenumbers when a substitution occurs for materials having low molar mass [24].

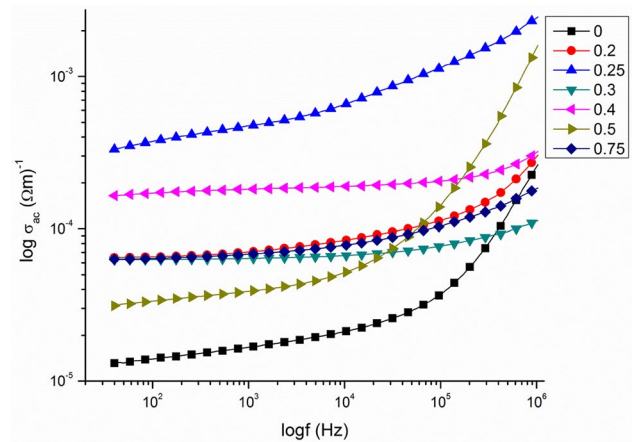


Fig. 5 Frequency-dependence of AC conductivity of the ionic conductors LAHP

3.4 Ionic conductivity

The AC conductivity (σ_{ac}) is one of the electrical parameters used to investigate and analyzed the dynamics of ions in polycrystalline materials such as NASICON compounds. The variations of AC conductivity (σ_{ac}) with frequency of un-substituted LHP and Al substituted LAHP at room temperature and within the frequency range 40 Hz to 1 MHz are depicted in Fig. 5. It is well known that AC conductivity, σ_{ac} of an ionic polycrystalline material at a certain temperature is always explained in terms of Jonscher's power law as described in Eq. (3) [10]. The plots in Fig. 5 give the variation of AC conductivity with frequency in the log scale. The conductivity is frequency-independent in the low frequency region. However, as frequency increases, the features of power law $\sigma(\omega)\omega^n$ are observed in the higher frequency region, where the AC conductivity is frequency dependent. The switch over behavior of AC conductivity from low frequency plateau region to higher frequency regime is an indication of an onset conductivity relaxation property of the as-prepared samples. The increasing trend of AC conductivity with increasing frequency is associated with the disorder of the Li cations within the sites. The presence of space charge also contributes to the increase in the conductivity. It is also observed that the un-substituted LHP pellet showed low AC conductivity in the order of $2.45 \times 10^{-4}\text{ }\Omega^{-1}\text{m}^{-1}$ at room temperature as reported elsewhere [16]. On the other hand, the Al substituted sintered pellets exhibited high Li ionic conductivity than the un-substituted LHP. The highest conductivity was observed in the sample with composition $x=0.25$ where $\sigma_{ac} = 2.5 \times 10^{-3}\text{ }\Omega^{-1}\text{m}^{-1}$. In a similar study, Morimoto et al. [25] investigated the lithium ionic conductivity of $\text{Li}_{1+x}\text{Al}_x\text{Ti}_{2-x}(\text{PO}_4)_3$ LATP with compositions $x=0, 0.3, 0.35, 0.4, 0.45, 0.5$ and 0.6 . The findings indicated

the un-substituted sample also showed low conductivity while the Al substituted samples indicated high lithium conductivity. According to the report, the sample with $x=0.45$ exhibited the highest ionic conductivity in the order of $2.9 \times 10^{-2} \Omega^{-1} \text{m}^{-1}$ at 25°C with activation energy of 30 KJ mol^{-1} [25]. In addition, the effect of Mn substitution on the conductivity of lithium titanium phosphate (LTP), $\text{LiMn}_x\text{Ti}_{2-x}(\text{PO}_4)_3$ ($x=0.0, 0.1, 0.3$ and 0.5) was also reported [26]. A low content of Mn yield high conductivity than those having high content of Mn. This is in accordance to the present results where low content of Al substitution exhibited higher AC conductivity.

Figure 6 shows the fitted Nyquist plots for the complex impedance of the as-prepared samples $\text{Li}_{1+x}\text{Al}_x\text{Hf}_{2-x}(\text{PO}_4)_3$

with $x=0, 0.2, 0.25, 0.3, 0.4, 0.5$ and 0.75 . The Nova software was used to analyze the equivalent circuits which differentiated the various effects of both grain-interior and grain boundary impedance. The plots were modeled based on the Nyquist plot with two parallel RC circuits combined in series. It is clearly seen from the analysis that the entire plots consist of two semicircles overlapping one another with a small tilted spike at the lowest frequency region. The semicircles at high frequency region correspond to the grain-interior impedance whereas the semicircles at low frequency correspond to the contribution of grain boundary impedance. Meanwhile, the semicircles are represented in Fig. 7 using the corresponding combination of resistances R_g , R_{gb} and capacitance which are

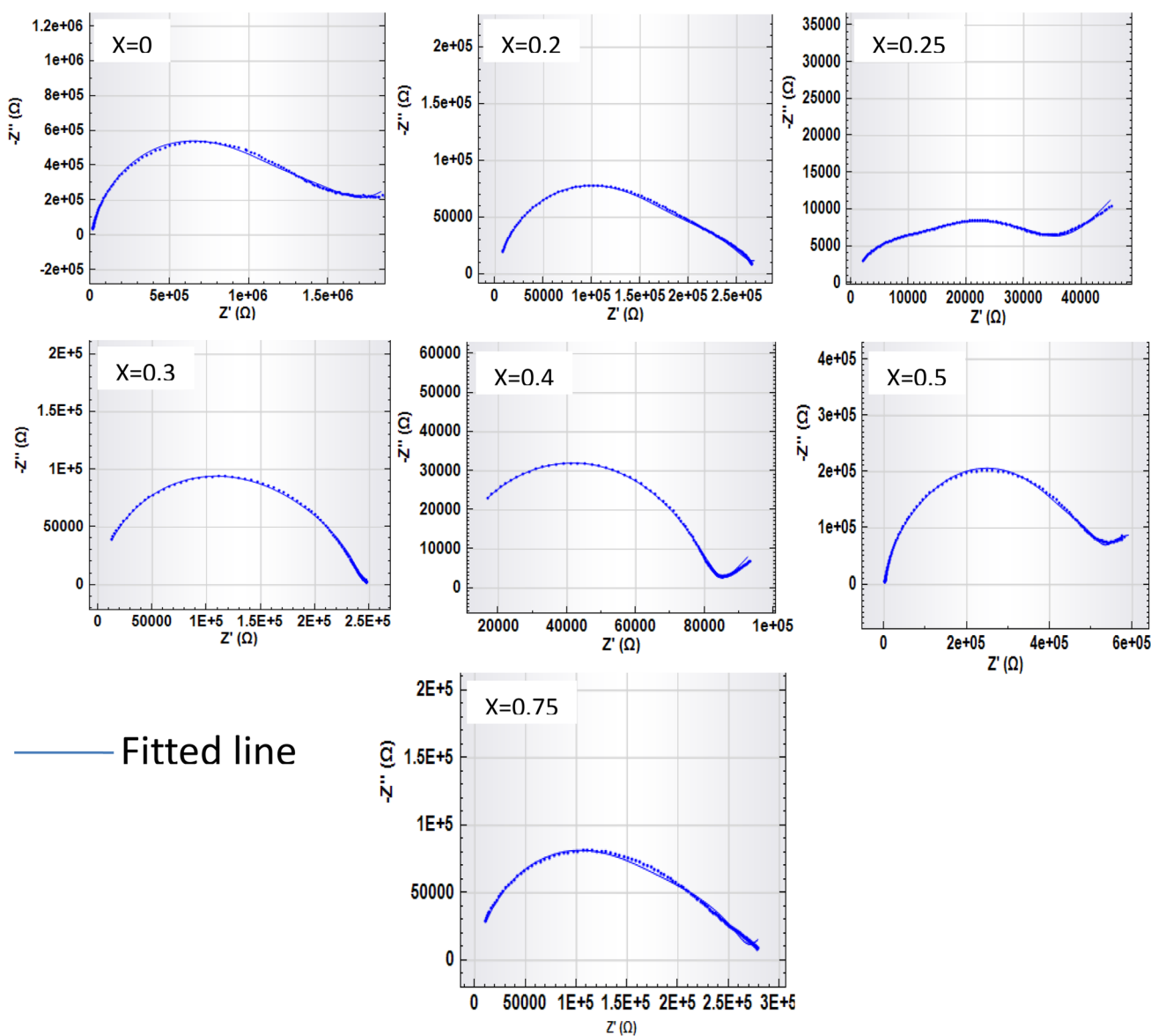


Fig. 6 Complex impedance Nyquist plots for the samples $\text{Li}_{1+x}\text{Al}_x\text{Hf}_{2-x}(\text{PO}_4)_3$ with $x=0, 0.2, 0.25, 0.3, 0.4, 0.5$ and 0.75

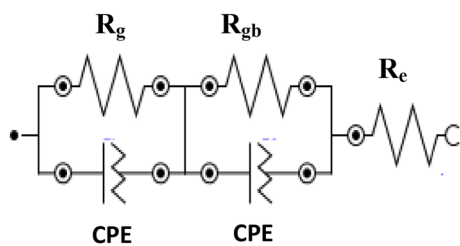


Fig. 7 Typical equivalent circuit model on the cores of impedance data for the various compositions of the LAHP

manage with the constant phase element (CPE). The CPE in the fitted circuit shows the presence of secondary phases or impurities in the samples as reported [27]. The parameters of equivalent circuit (R_g and R_{gb}), the conductivities (σ_g and σ_{gb}) and the estimated measurement accuracy (Chi square (χ^2) values) of the LAHP with their corresponding dimensions are tabulated in Table 3. It is observed that the un-substituted LHP exhibited high resistance for both grain and grain boundary impedance with low DC conductivity as shown in Table 3. However, high DC conductivity for both grain (σ_g) and grain boundary (σ_{gb}) was observed for the x substituted LAHP which is probably attributed to the increase in the Li^+ ion concentration from the Li_2CO_3 . The present analysis indicated LAHP with $x=0.25$ showed the highest grain boundary conductivity $\sigma_{gb} = 2.08 \times 10^{-3} (\Omega m)^{-1}$ with low activation energy of 0.36 eV as tabulated in Table 3. In a similar investigation, Chang [6] reported high Li conductivity for $x=0.5$ in LAHP analysis prepared via the spark plasma synthesis method ($1.1 \times 10^{-2} (\Omega m)^{-1}$) [6]. The report identified that the high conductivity is due to the Al substitution and increase in the lithium content improve the densification of the samples. The substitution of Fe into LHP was also reported resulting in high ionic conductivity ($1.7 \times 10^{-2} (\Omega m)^{-1}$) for $Li_{1.2}Fe_{0.2}Hf_{1.8}(PO_4)$ [28].

The temperature dependence of the grain boundary conductivity is depicted in Fig. 8 for $x=0.25$. The temperature dependence of the material was investigated using the Arrhenius plot. The Arrhenius equation is given by Eq. (8). The plot of Fig. 8 ($\ln \sigma$ vs. reciprocal temperature

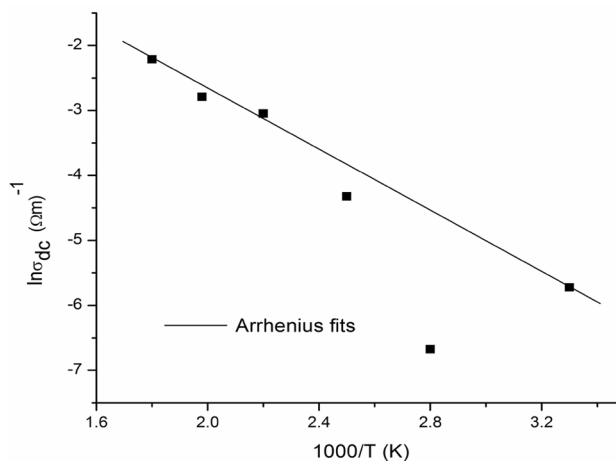


Fig. 8 Arrhenius plot for the temperature dependence of DC conductivity of grain-boundary for the LAHP with composition $x=0.25$

$1000/T$) together with Eq. 8 was used to calculate the activation energy of Li ion which is 0.36 eV.

4 Conclusion

The thermal decomposition behaviour and stability properties of the chemical reaction mixtures; lithium aluminum hafnium phosphate (LAHP) with various compositions ($x=0, 0.2, 0.25, 0.3, 0.4, 0.5$ and 0.75) were established using TGA/DTG. XRD and FTIR identified the various phases and composition in the as-prepared LAHP. The TGA results indicated systematic substitution and increase in the x content in the lithium aluminum hafnium phosphate (LAHP) reaction mixtures leads to the sample formation towards higher temperatures. The percentage mass loss and stability temperature of the reaction mixture increase as the x content is increased from $x=0$ to 0.75 . This is confirmed by shifting the DTG peaks to higher temperature. The XRD analysis confirmed the sample formation with hexagonal crystal axis belonging to R-3c space group with ICSD database 98-004-0755. The Rietveld refinement

Table 3 Parameters of Equivalent circuit, conductivity and χ^2 values for the LAHP including the dimensions (thickness, t and area, A)

Sample (x)	Dimension		$R_g (\Omega)$	$R_{gb} (\Omega)$	χ^2	$\sigma_{dcg} (\Omega m)^{-1}$	$\sigma_{dcgb} (\Omega m)^{-1}$
	t	A					
0	1.95E-03	7.85E-05	8.40E+05	8.50E+05	0.050	2.94E-05	2.90E-05
0.2	2.05E-03	1.19E-04	1.42E+05	1.14E+05	0.012	1.21E-04	1.51E-04
0.25	1.89E-03	1.17E-04	2.70E+04	7.76E+03	0.005	5.98E-04	2.08E-03
0.3	1.80E-03	1.16E-04	1.60E+05	8.20E+04	0.008	9.70E-05	1.89E-04
0.4	1.85E-03	1.19E-04	4.90E+04	3.60E+04	0.030	4.57E-05	2.83E-04
0.5	2.07E-03	1.10E-04	3.40E+05	5.50E+04	0.029	1.25E-04	1.65E-04
0.75	1.86E-03	1.06E-04	1.50E+05	1.14E+05	0.035	1.17E-04	1.54E-04

analysis indicated single phase in the un-substituted LHP, but for the Al substituted LAHP, various phases were observed as Al content increases. The vibrational and stretching modes of PO_4 of LAHP were observed and confirmed by the FTIR spectra. For the electrical analysis, the un-substituted LHP showed low AC and estimated DC conductivity, but with increase in x -content and Al substitution, the conductivity is enhanced. For the present analysis, $\text{Li}_{1+x}\text{Al}_x\text{Hf}_{2-x}(\text{PO}_4)_3$ with $x=0.25$ was observed having high Li ionic conductivity, $\sigma=2.5 \times 10^{-3} \Omega^{-1}\text{m}^{-1}$ and low activation energy of 0.36 eV. It is concluded that low concentrations of Al in LAHP is more effective than high content of Al substitution. The present studies suggest that $\text{Li}_{1.25}\text{Al}_{0.25}\text{Hf}_{1.75}(\text{PO}_4)_3$ can be a future promising solid electrolyte material for application in solid-state batteries.

Acknowledgements The authors gratefully acknowledge Department of Physics, Faculty of Science, Universiti Putra Malaysia (UPM) for the facilities provided.

Funding This research work was supported financially by the Ministry of Education Malaysia through the Fundamental Research Grant Scheme (FRGS) Project No. 01-02-14-1599FR.

Compliance with ethical standards

Conflict of interest The authors declare that they have no conflict of interest.

References

- Mouahid FE, Zahir M, Maldonado-manso P, Bruque S, Losilla ER, Chimie D, Doukkali C, Jadida E (2001) Na–Li exchange of $\text{Na}_{1+x}\text{Ti}_{2-x}\text{Al}_x(\text{PO}_4)_3$ ($0.6 < x < 0.9$) NASICON series: a Rietveld and impedance study. *J Mater Chem* 3:3258–3263
- Petkov VI, Orlova AI, Egorkova OV (1996) On the existence of phases with a structure of $\text{NaZr}_2(\text{PO}_4)_3$ in series of binary orthophosphates with different alkaline element to zirconium ratios. *J Struct Chem* 37:933–940
- Aono H (1990) Ionic conductivity and sinterability of lithium titanium phosphate system. *Solid State Ion* 40–41:38–42
- Maldonado-manso P, Losilla ER, Aranda MAG, Mouahid FE, Zahir M (2003) High, lithium ionic conductivity in the $\text{Li}_{1+x}\text{Al}_x\text{Ge}_y\text{Ti}_{2-x-y}(\text{PO}_4)_3$ NASICON series. *Chem Mater* 15:1879–1885
- Thangadurai V, Shukla AK, Gopalakrishnan J (1999) New lithium-ion conductors based on the NASICON structure. *J Mater Chem* 9:739–741
- Chang C-M, Hong S-H, Park H-M (2005) Spark plasma sintering of Al substituted $\text{LiHf}_2(\text{PO}_4)_3$ Solid electrolytes. *Solid State Ion* 176:2583–2587
- Losilla ER, Aranda MAG, Martínez-Lara M, Bruque S (1997) Reversible triclinic-rhombohedral phase transition in $\text{LiHf}_2(\text{PO}_4)_3$: crystal structures from neutron powder diffraction. *Chem Mater* 9:1678–1685
- Losilla ER, Aranda MAG, Bruque S, Quarton S (2000) Sodium mobility in the NASICON series $\text{Na}_{1+x}\text{Zr}_{2-x}\text{In}_x(\text{PO}_4)_3$. *Chem Mater* 12:2134–2142
- Ahmadu U, Musa AO, Jonah SA, Rabiun N (2010) Synthesis and thermal characterization of NZP compounds. *J Therm Anal Calorim* 2:175–179
- Halim ZA, Adnan SBRS, Mohamed NS (2016) Effect of sintering temperature on the structural, electrical and electrochemical properties of novel $\text{Mg}_{0.5}\text{Si}_2(\text{PO}_4)_3$ ceramic electrolytes. *Ceram Int* 42:4452–4461
- Savitha T, Selvasekarapandian S, Ramya CS, Bhuvaneshwari MS, Angelo APC (2007) Electrical conduction and relaxation mechanism in $\text{Li}_2\text{AlZr}(\text{PO}_4)_3$. *J Mater Sci* 42:5470–5475
- Key B, Schroeder DJ, Ingram BJ, Vaughey JT (2012) Solution-based synthesis and characterization of lithium-ion conducting phosphate ceramics for lithium metal batteries. *Chem Mater* 24:287–293
- Ignaszak A, Pasierb P, Gajerski R, Komornicki S (2005) Synthesis and properties of Nasicon-type materials. *Thermochim Acta* 426:7–14
- Losillaa ER, Bruquea S, Arandaa MAG, Moreno-Real L, Morin E, Quarton M (1998) NASICON to scandium wolframate transition in $\text{LiMHf}(\text{PO}_4)_3$ ($M = \text{Cr, Fe}$): structure and ionic conductivity. *Solid State Ion* 112:53–62
- Naik AH, Thakkar NV, Dharwadkar SR, Singh Mudher KD, Vengopal V (2004) Microwave assisted. *J Therm Anal Calorim* 78:707–713
- Zangina T, Hassan J, Azis RS (2018) Structural, electrical conductivity and dielectric relaxation behavior of $\text{LiHf}_2(\text{PO}_4)_3$ ceramic powders. *J Aust Ceram Soc* 54:307–316. <https://doi.org/10.1007/s41779-017-0155-2>
- París MA, Martínez-Juárez A, Iglesias JE, Rojo JM, Sanz J (1997) Phase transition and ionic mobility in $\text{LiHf}_2(\text{PO}_4)_3$ with NASICON structure. *Chem Mater* 9:1430–1436
- Martínez-Juárez A, Amarilla JM, Iglesias JE, Rojo JM (1997) Ionic conductivity of $\text{LiHf}_2(\text{PO}_4)_3$ with NASICON-type structure and its possible application as electrolyte lithium batteries. *J Braz Chem Soc* 8:261–264
- Winand J-M, Rulmont A, Tarte P (1991) Nouvelles solutions solides $\text{Li}(\text{MIV})_{2-x}(\text{NIV})_x(\text{PO}_4)_3$ ($L = \text{Li, Na, M, N} = \text{Ge, Sn, Ti, Zr, Hf}$) synthèse et étude par diffraction x et conductivité ionique. *J Solid State Chem* 93:341–349
- Corbridge D (1956) The crystal structure of magnesium phosphate hexahydrate, $\text{MgHPO}_3 \cdot 6\text{H}_2\text{O}$. *Acta Crystallogr* 9:991–994
- Sun F, Wang R, Heng J, Weilei Z (2013) Synthesis of sodium titanium phosphate at ultra- low temperature. *Res Chem Intermed* 39:1857–1864
- Anuar NK, Adnan SBRS, Muhamed NS (2014) Characterization of $\text{Mg}_{0.5}\text{Zr}_2(\text{PO}_4)_3$ for potential use as electrolyte in solid state magnesium batteries. *Ceram Int* 40:13719
- Mustaffa NA, Adnan SBRS, Sulaiman M, Mohamed NS (1995) Low-temperature effects on NASICONstructured $\text{LiSn}_2\text{P}_3\text{O}_{12}$ solid electrolytes prepared via citric acid- assisted sol-gel method. *Ionics* 21:955–965
- Skaudzius R, Pinkas J, Raudonis R, Selskis A, Juskenas R, Kareiva A (2012) On the ionic radius of garnet structure compounds $\text{Y}_3\text{Al}_5-x\text{M}_x\text{O}_{12}$ ($M = \frac{1}{4} \text{Cr, Co, Mn, Ni, Cu}$) and $\text{Y}_3\text{Fe}_5-x\text{Co}_x\text{O}_{12}$ ($0 < x < 2.75$) synthesized by sol-gel method. *Mater Chem Phys* 135:479–485
- Morimoto H, Hirukawa M, Matsumoto A, Kurahayashi T (2014) Nobukiyo ITO, and shin-ichi tobishima, lithium ion conductivities of NASICON-type $\text{Li}_{1+x}\text{Al}_x\text{Ti}_{2-x}(\text{PO}_4)_3$ solid electrolytes prepared from amorphous powder using a mechanochemical method. *Electrochemistry* 82:870
- Venkateswara Rao A, Veeraiaha V, Prasada Rao AV, Kishore Babu B (2013) Effect of Mn substitution on the electrochemical properties of $\text{LiTi}_2(\text{PO}_4)_3$. *Chem Sci Trans* 2:105–112

27. Kothari DH, Kanchan DK (2015) Study of Study of electrical properties of gallium-doped lithium titanium aluminum phosphate compounds. *Ionics* 21:1253–1259
28. Aono H, Sugimoto E, Sadaoka Y, Imanaka N, Adachi G-Y (1993) Electrical properties and crystal structure of solid electrolyte based on lithium hafnium phosphste $\text{LiHf}_2(\text{PO}_4)_3$. *Solid State Ion* 62:309–316

Publisher's Note Springer Nature remains neutral with regard to jurisdictional claims in published maps and institutional affiliations.